J. Plasma Physics (2002), *vol.* 68, *part* 1, *pp.* 27–52.
DOI: 10.1017/S0022377802001745 Printed in the United Kingdom

Solitons and oscillitons in cold bi-ion plasmas: a parameter study

E. DUBININ,[1] K. SAUER[1] and J. F. McKENZIE[1,2]

[1]Max-Planck Institut für Aeronomie, Katlenburg – Lindau, Germany

[2]School of Pure and Applied Physics, University of Natal, Durban, South Africa

(Received 30 January 2002)

Abstract. We investigate the structure of nonlinear stationary waves propagating obliquely to the magnetic field in a cold bi-ion plasma. By using the constants of motion that follow from the multifluid equations, the system may be described by four coupled first-order differential equations. A new constant of motion characterizing a bi-ion flow (called the 'energy difference integral') is found. The combination of relations between the flow speeds derived from the conservation laws, which we call the 'momentum–energy hodographs', reveal some important features of stationary waves and solitons. Soliton solutions representing both compressions and rarefactions in the ion fluids exist in specific windows in the 'Alfvén Mach number–obliquity' space. In other windows, solutions characterized by both oscillating and soliton properties ('oscillitons') exist. Critical Mach numbers and propagation angles narrow the size of the windows where smooth soliton solutions can be constructed.

1. Introduction

Nonlinear stationary waves in bi-ion plasmas have attracted considerable attention in recent years – essentially because of the multi-ion nature of many space plasmas (Verheest 1990; Hackenberg et al. 1998; Sauer et al. 2000, 2001, 2002a, b; McKenzie et al. 2001; Dubinin et al. 2002). Using expansion techniques, Verheest (1990) obtained a derivative nonlinear Schrödinger equation describing Alfvén solitons propagating parallel to the magnetic field in a differentially streaming bi-ion plasma. This weakly nonlinear treatment permits a study of the evolution and stability of such stationary structures. A fully nonlinear approach was adopted by Dubinin et al. (2002) to investigate the properties of transverse stationary waves and solitons in a bi-ion plasma. The conservation laws, derived from the multi-ion fluid equations, enable the system to be described by a first-order differential equation (the structure equation that permits a detailed analysis of the phase trajectories of the dynamic system). In the case of oblique propagation, such a fully nonlinear approach was also developed for a proton–electron plasma, where the energy integral of the system yields a first-order differential equation for the structure (McKenzie & Doyle 2001).

In this paper, we examine the structure of stationary waves propagating obliquely to the ambient magnetic field in a bi-ion plasma. The paper is organized as follows. In Sec. 2, we set up governing equations, which are the multifluid equations for each

species (and the approximation of massless electrons), along with the Maxwell equations. There are several constants of motion that simplify the system of equations. The continuity equations relate the number densities of ion species and electrons to their velocity components in the direction of wave propagation (the x axis). Conservation of the components of the momentum flux yields three relations between the flow speeds and the magnetic field components. Using transverse momentum conservation, the two magnetic field components are expressed in terms of the transverse speeds (and, of course, B_x is constant because of Gauss' law). Faraday's law for stationary flows yields the conservation of two transverse components of the electric field. Using these together with x-momentum conservation and energy flux conservation, the speeds of both ion species in the direction of wave propagation may also be expressed in terms of their transverse components. The remaining equations are four coupled differential equations of first order for the transverse speeds. These equations together with the constants of motion completely describe the dynamic system. We also derive another integral of the motion, which we call the 'energy difference integral' and which, together with the energy flux integral, gives insight into some of the properties of stationary waves without recourse to solving differential equations. In Sec. 3, we analyse these algebraic relations between ion speeds (called 'the momentum–energy hodographs') in more detail. It is shown that throughout any stationary wave, the components of the velocity of both protons and heavies lie on the surface of a sphere whose position and radius are determined by the obliquity of the wave.

The dispersion equation for stationary waves is derived in Sec. 4 by linearizing the nonlinear coupled equations for the transverse speeds. Because of the decoupling of the equations for two transverse components, a necessary condition for evanescent (i.e. exponentially growing or decaying) solutions is reduced to finding the roots of the biquadratic characteristic equation for the wavenumber κ (a similar equation was deduced by Hackenberg et al. 1998). The roots of this equation yield the ranges of the Alfvén Mach numbers and obliquities in which soliton solutions can be constructed. In addition to the 'classical' soliton solution, we find a new type of stationary wave (called an 'oscilliton'), characterized by an oscillating structure superimposed on the spatial growth or decay (Sauer et al. 2001, 2002a, b).

In Sec. 5, we present typical structures of solitons and oscillitons, and show how they vary with different parameters. Both compressive and rarefactive solitons are found. In Sec. 6, we discuss the problem of critical Mach numbers. In compressive solitons, the critical Mach number corresponds to a 'stagnation' of the heavy-ion flow, while the proton speed remains finite.

2. Governing equations and conservation laws

The standard multifluid equations for a cold bi-ion plasma (protons p and heavy ions h) are

$$\frac{\partial n_i}{\partial t} + \boldsymbol{\nabla} \cdot (n_i \mathbf{u}_i) = 0, \tag{1}$$

$$m_i n_i \frac{D_i \mathbf{u}_i}{Dt} = e n_i q_i (\mathbf{E} + \mathbf{u}_i \times \mathbf{B}), \tag{2}$$

where m_i is the mass, q_i the ion charge and n_i the number density of each species ($i = p, h$); $\mathbf{B}$ and $\mathbf{E}$ are the magnetic and electric field respectively, and the convective

https://doi.org/10.1017/S0022377802001745 Published online by Cambridge University Press

derivative is

$$\frac{D_i}{Dt} = \frac{\partial}{\partial t} + \mathbf{u}_i \cdot \boldsymbol{\nabla}. \tag{3}$$

For time scales much longer than the electron gyroperiod, electron inertia in negligible (massless electrons) and the electric field is given by

$$\mathbf{E} = -\mathbf{u}_e \times \mathbf{B}, \tag{4}$$

so that Faraday's law becomes

$$\frac{\partial \mathbf{B}}{\partial t} = \boldsymbol{\nabla} \times (\mathbf{u}_e \times \mathbf{B}). \tag{5}$$

The remaining equation, Ampère's law, is

$$\boldsymbol{\nabla} \times \mathbf{B} = \mu_o \mathbf{j}, \tag{6}$$

in which we neglect the displacement current and the current $\mathbf{j}$ is given by

$$\mathbf{j} = \sum_{i=p,h} e q_i n_i \mathbf{u}_i - e n_e \mathbf{u}_e. \tag{7}$$

Here we consider stationary ($\partial/\partial t = 0$) structures propagating in the x direction ($D/Dt = u_i d/dx$) in a bi-ion plasma, which in this frame appears to flow obliquely to the magnetic field $\mathbf{B} = (B_x, 0, B_{z0})$. The number flux of each species is constant:

$$n_i u_{ix} = f_i = \text{const}. \tag{8}$$

Adding the x, y and z components of the equations of motion (2) for ions and electrons (with $m_e = 0$) and integrating yields the total momentum conservation equations in the x, y and z directions:

$$\sum_{i=p,h} m_i f_i u_{ix} + \frac{B_y^2 + B_z^2}{2\mu_0} = \text{const}, \tag{9}$$

$$\sum_{i=p,h} m_i f_i u_{iy} - \frac{B_x B_y}{\mu_0} = \text{const}, \tag{10}$$

$$\sum_{i=p,h} m_i f_i u_{iz} - \frac{B_x B_z}{\mu_0} = \text{const}, \tag{11}$$

in which the conditions of quasineutrality ($n_p + n_h = n_e$) and current-free flow ($j_x = e(n_p u_{px} + n_h u_{hx} - n_e u_{ex}) = 0$) have also been used.

Multiplying the x, y and z components of the equations of motion (2) by $u_{px}(u_{hx})$, $u_{py}(u_{hy})$ and $u_{pz}(u_{hz})$ and adding them yields, after integration, conservation of the energy flux:

$$\sum_{i=p,h} f_i \frac{m_i(u_{ix}^2 + u_{iy}^2 + u_{iz}^2)}{2} + \frac{(\mathbf{E} \times \mathbf{B})_x}{\mu_0} = \text{const}. \tag{12}$$

https://doi.org/10.1017/S0022377802001745 Published online by Cambridge University Press

For stationary structures, $\nabla \times \mathbf{E} = 0$, which gives conservation of the transverse electric field:

$$E_y = \text{const}, \qquad E_z = \text{const}. \tag{13}$$

Equations (8)–(13) represent the important conserved quantities of number flux, momentum flux, energy flux and transverse electric field. For convenience, we normalize these equations, assuming that at $x = -\infty$, $n_p = n_{p0} = 1$, $n_h = n_{h0} = \alpha$ (where α is the ion abundance), $u_{ix} = u_0 = 1$, and $B = B_0 = 1$, $B_{x0} = \cos\theta$, $B_{z0} = \sin\theta$, $u_{py0} = u_{pz0} = u_{hy0} = u_{hz0} = 0$ (where θ is the angle between the x axis and the magnetic field B_0), and they then become

$$f_p = 1, \qquad f_h = \alpha, \qquad f_e = 1 + \alpha, \tag{14}$$

$$u_{px} - 1 + \alpha\mu(u_{hx} - 1) + \frac{1}{2M_A^2}(B_y^2 + B_z^2 - \sin\theta^2) = 0, \tag{15}$$

$$u_{py} + \alpha\mu u_{hy} - \frac{B_x B_y}{M_A^2} = 0, \tag{16}$$

$$u_{pz} + \alpha\mu u_{hz} - \frac{B_x(B_z - \sin\theta)}{M_A^2} = 0, \tag{17}$$

$$u_{px}^2 - 1 + \alpha\mu(u_{hx}^2 - 1) + (u_{py}^2 + u_{pz}^2) + \alpha\mu(u_{hy}^2 + u_{hz}^2) + \frac{2E_y(B_z - \sin\theta)}{M_A^2} = 0, \tag{18}$$

where $\mu = m_h/m_p$ and $M_A = u_0/V_{Ap}$ are respectively the mass ratio and the Alfvén Mach number ($V_{Ap} = B_0/(\mu_0 n_{p0} m_p)^{1/2}$ is the Alfvén speed based on the proton mass density). Note also that $E_y = u_e B_{z0} = \sin\theta$, $E_z = 0$ and $B_x = \cos\theta$. Using these equations, we may express B_y, B_z and u_{px}, u_{hx} as functions of the transverse velocity components of the protons and the heavies. The remaining equations, which close the system, are the differential equations of motion for the transverse velocities u_{py}, u_{pz}, u_{hy} and u_{hz}:

$$u_{px}\frac{du_{py}}{dx} = E_y + u_{pz}B_x - u_{px}B_z, \tag{19a}$$

$$u_{px}\frac{du_{pz}}{dx} = u_{px}B_y - u_{py}B_x, \tag{19b}$$

$$\mu u_{hx}\frac{du_{hy}}{dx} = E_y + u_{hz}B_x - u_{hx}B_z, \tag{20a}$$

$$\mu u_{hx}\frac{du_{hz}}{dx} = u_{hx}B_y - u_{hy}B_x. \tag{20b}$$

Here the x variable is normalized to the value u_0/Ω_p, where $\Omega_p = eB_0/m_p$ is the proton gyrofrequency, and $q = 1$.

Before analysing this set of equations (19)–(20), together with the constants of motion (8)–(11), we note that there is a further conservation law that, combined with the others, allows us to elucidate some features of stationary waves. This relation is obtained by multiplying (19) and (20) by u_{py}, u_{pz} and u_{hy}, u_{hz} respectively, using the x equations of motion (2) in the normalized form, and collecting the terms in pairs

$$\mu u_{hx}\frac{du_{hx}}{dx} - u_{px}\frac{du_{px}}{dx}, \qquad \mu u_{hy}\frac{du_{hy}}{dx} - u_{py}\frac{du_{py}}{dx}, \qquad \mu u_{hz}\frac{du_{hz}}{dx} - u_{pz}\frac{du_{pz}}{dx}.$$

https://doi.org/10.1017/S0022377802001745 Published online by Cambridge University Press

After adding, this yields

$$\frac{\mu}{2}\frac{d}{dx}(u_{hx}^2+u_{hy}^2+u_{hz}^2)-\frac{1}{2}\frac{d}{dx}(u_{px}^2+u_{py}^2+u_{pz}^2)+\frac{E_y}{B_x}\left(\mu\frac{du_{hz}}{dx}-\frac{du_{pz}}{dx}\right)=0, \quad (21)$$

which, on integration, gives

$$\mu(u_{hx}^2-1)-(u_{px}^2-1)+\mu(u_{hy}^2+u_{hz}^2)-(u_{py}^2+u_{pz}^2)+\frac{2E_y}{B_x}(\mu u_{hz}-u_{pz})=0. \quad (22)$$

We call this the 'energy difference integral'. On eliminating the u_{hx}^2 term from (22) using energy flux conservation (18), we obtain

$$u_{px}^2+u_{py}^2+\left(u_{pz}+\frac{E_y}{B_x}\right)^2=1+\left(\frac{E_y}{B_x}\right)^2=R_E^2, \quad \text{say.} \quad (23)$$

Similarly, elimination of the u_{px}^2 term leads to

$$u_{hx}^2+u_{hy}^2+\left(u_{hz}+\frac{E_y}{B_x}\right)^2=1+\left(\frac{E_y}{B_x}\right)^2=R_E^2. \quad (24)$$

Thus, throughout the wave, we have the remarkable result that the components of the velocities of both protons and heavies lie on the surface of a sphere of radius R_E whose centre is at $(0, 0, -E_y/B_x)$ and on which the initial point is $(1, 0, 0)$.

3. Momentum–energy hodographs

Recently McKenzie et al. (2001) and Dubinin et al. (2002) showed that many features of bi-ion plasma flows transverse to the magnetic field can be deduced from the constants of motion. Using momentum flux conservation in the x direction and charge neutrality, one can derive an algebraic relation, called the momentum hodograph, between the ion speeds and the magnetic field in stationary structures. Using together with these the energy flux integral (the analogue of the Rankine–Hugoniot relations), one can find amplitudes of solitons as functions of the Mach number. In the oblique case, the picture becomes more complicated because of the appearance of several new variables (u_{py}, u_{pz}, u_{hy}, u_{hz}, B_y, B_z). Nevertheless, a combined analysis of the conservation laws permits us to predict some important features of stationary waves by providing us with relations between the ion speeds, which we term the 'momentum–energy hodographs'. As already mentioned, the energy flux and energy difference integrals (23) and (24) represent in $\mathbf{u}_i$ space a sphere of radius R_E displaced from the origin along the u_{iz} axis by $-E_y/B_x$ units (Fig. 1). The system evolves from the initial point O where u_i = (1, 0, 0) and each $\mathbf{u}_i$ 'moves' along some path on the same spherical surface. It is important to note that the phase trajectories of the protons and the heavies on this sphere may be different. Thus 'downward' or 'upward' movement from the initial point over the sphere leads to compressional or expansional solutions. The maximum possible compression of the system is reached if one of the ion speeds (u_{px} or u_{hx}) approaches zero. This point (C_m) corresponds to the appearance of a critical Mach number. A priori, it is not possible to predict which field (or both together) reaches this critical point. The maximum possible rarefaction in ion flows is determined by the 'top' point on the sphere (R_m), where u_{px} or u_{hx} equals $\sqrt{1+E_y^2/B_x^2}$ and u_{pz} (or u_{hz}) $= -E_y/B_x$. This implies that the maximum rarefaction increases as the obliquity $\sim \tan\theta$.

https://doi.org/10.1017/S0022377802001745 Published online by Cambridge University Press

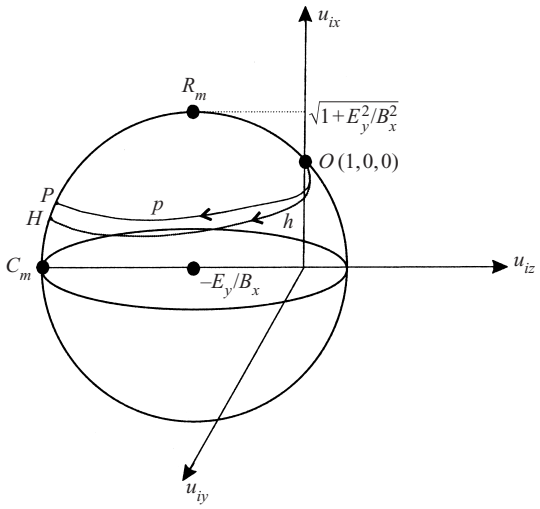

Figure 1. In bi-ion stationary flows oblique to the ambient magnetic field, the tip of the proton (heavy-ion) flow velocity vector moves on the surface of a sphere of radius $R_E = \sqrt{1 + E_y^2/B_x^2}$, displaced from the origin along the $u_{pz,hz}$ axis by $-E_y/B_x$ units. Downward and upward motions from the initial point O $(1, 0, 0)$ correspond to compressive and rarefactive flows respectively. Two possible trajectories of the p, h tips that describe a structure of a compressive soliton are shown. The proton (heavy-ion) flow velocity vector reaches the point $P(H)$ in the centre of the structure and moves back to the initial point O along a symmetrical trajectory on the opposite side of the sphere. The point C_m corresponds to the appearance of a critical Mach number for compressive flows. The point R_m determines the maximum possible rarefaction.

The other constraints are x-momentum flux, energy flux and energy density difference conservations, which may be written as

$$u_{px} + \alpha\mu u_{hx} = R_1, \tag{25a}$$

$$u_{px}^2 + \alpha\mu u_{hx}^2 = R_2^2, \tag{25b}$$

$$\mu u_{hx}^2 - u_{px}^2 = R_3^2, \tag{25c}$$

where R_1, R_2 and R_3 are functions only of the ion transverse speeds, which follow readily from (15), (18) and (22). Note that R_2^2 is always a positive quantity, whereas R_3^2 as a function of transverse speeds may switch sign. Thus, in the (u_{hx}, u_{px}) plane, the curves are the 'momentum' straight line through the points $(0, R_1)$ and $(R_1/\alpha\mu, 0)$, the 'energy flux' ellipse with semiaxes $R_2/\sqrt{\alpha\mu}$ and R_2, and the 'energy difference' hyperbola with real axis $2R_3/\sqrt{\mu}$, all of which intersect at the 'initial' point O of the system $u_{px} = u_{hx} = 1$ (Fig. 2a). The curves then evolve by contracting or expanding, while the point (u_{px}, u_{hx}), which corresponds to a bi-ion stationary flow, remains at the intersection of these characteristic curves: the momentum flux (solid), energy flux (dashed) and energy density (dotted) curves (Figs 2b, c). Note that initially the 'momentum curve' is tangent to the 'energy flux' curve (ellipse) at $u_{ix} = 1$. In general, there are two roots, which can be found, for example, by

https://doi.org/10.1017/S0022377802001745 Published online by Cambridge University Press

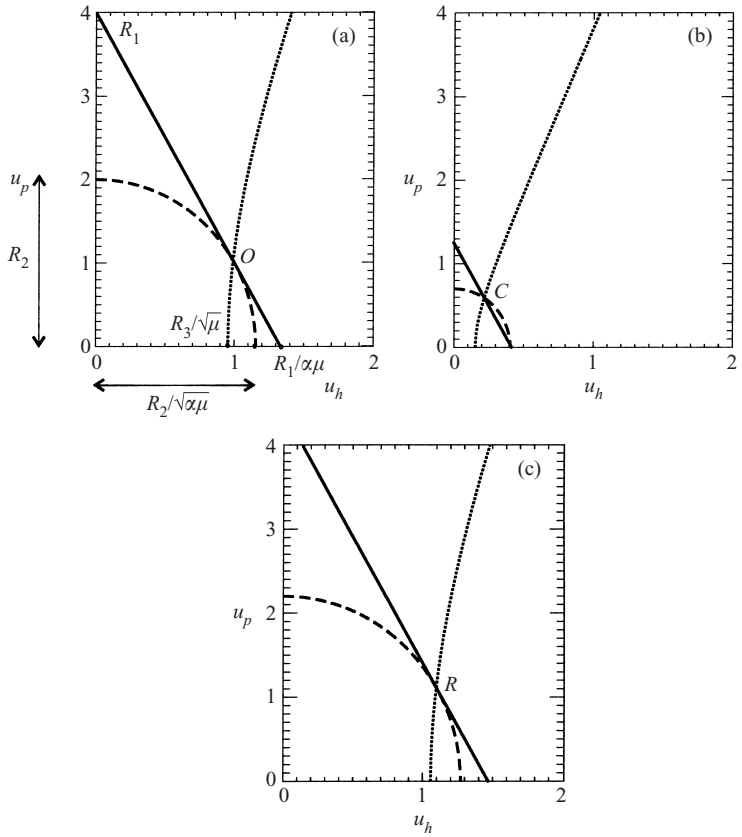

Figure 2. Intersection of the three curves that represent geometrically the conservation of momentum flux (straight solid line), energy flux (dashed ellipse) and energy difference (dotted hyperbola), corresponds to the state of the system in a stationary wave. The point O corresponds to the initial state of the system. The points C and R correspond to the state at the centre of a compressive and a rarefactive soliton respectively.

solving (25a, b) and are given by

$$u_{hx} = \frac{R_1\sqrt{\alpha\mu} \mp \sqrt{R_2^2(1+\alpha\mu) - R_1^2}}{\sqrt{\alpha\mu}(1+\alpha\mu)}, \tag{26a}$$

$$u_{px} = \frac{R_1\sqrt{\alpha\mu} \pm \alpha\mu\sqrt{R_2^2(1+\alpha\mu) - R_1^2}}{\sqrt{\alpha\mu}(1+\alpha\mu)}, \tag{26b}$$

where the upper and lower signs correspond respectively to compressive and rarefaction structures, obtained from numerical solutions of the equations of motion. In compressive flows (where the value $u_{px}^2 + \alpha\mu u_{hx}^2$ decreases), the ellipse contracts and the intersection point C moves to the left (Fig. 2b) and, generally speaking, may reach the point $u_{hx} = 0$ while u_{px} remains finite. In expansion flows, the ellipse expands and the point R moves to the right (Fig. 2c). In this case, one may expect the expansion in the proton flow to reach a maximum value and then decrease ($u_{px} \to 1$), leaving an expansion in the heavy flow. Similar characteristic curves may be plotted for the transverse variables u_{pz} and u_{hz}. However, these momentum–energy hodographs alone do not determine the position of the 'equi-

https://doi.org/10.1017/S0022377802001745 Published online by Cambridge University Press

librium point' (from which the system evolves back to the initial point), which can only be found from solution of the system of nonlinear differential equations (19) and (20).

4. Stationary-wave dispersion equation

The system of equations (19) and (20), written in the vector form

$$\frac{du_j}{dx} = f_j(u_k, c_j), \tag{27}$$

where u_j are the transverse speed components ($j,k = py, pz, hy, hz$) and c_j are constants, can be linearized in the neighbourhood of the initial point ($u_{px} = u_{hx} = 1$, $u_j = 0$, $B_y = 0$, $B_x = \cos\theta$, $B_z = \sin\theta$, $E_y = \sin\theta$) to give

$$\frac{du_j}{dx} = f_j(u_k = 0, c_j) + \left(\frac{\partial f_j}{\partial u_k}\right)_{u_k=0} u_k = \left(\frac{\partial f_j}{\partial u_k}\right)_{u_k=0} u_k. \tag{28}$$

Evanescent solutions $\sim \exp(\kappa x)$ yield the matrix equation

$$(\hat{\mathbf{L}} - \kappa\hat{\mathbf{I}})\mathbf{u} = 0, \tag{29}$$

which has non-trivial solutions if and only if

$$\det(\hat{\mathbf{L}} - \kappa\hat{\mathbf{I}}) = 0. \tag{30}$$

Here $\hat{\mathbf{I}}$ is the unit matrix and $L_{jk} = (\partial f_j/\partial u_k)_{u_k=0}$:

$$\mathbf{L} = \begin{pmatrix} 0 & \dfrac{1-M_A^2}{\cos\theta} & 0 & \dfrac{\alpha\mu M_A^2}{\cos\theta} \\ \dfrac{M_A^2}{\cos\theta} - \cos\theta & 0 & \dfrac{\alpha\mu M_A^2}{\cos\theta} & 0 \\ 0 & -\dfrac{M_A^2}{\mu\cos\theta} & 0 & \dfrac{1-\alpha\mu M_A^2}{\mu\cos\theta} \\ \dfrac{M_A^2}{\mu\cos\theta} & 0 & \dfrac{\alpha\mu M_A^2 - \cos^2\theta}{\mu\cos\theta} & 0 \end{pmatrix}$$

Note that in linearizing (19) and (20) we have used (23) and (24) to obtain the perturbations in the longitudinal velocities, $\delta u_{px} = -u_{pz}\tan\theta$ and $\delta u_{hx} = -u_{hz}\tan\theta$. The characteristic equation is a biquadratic of the form

$$A\kappa^4 + B\kappa^2 + C = 0. \tag{31}$$

Before analysing this equation, note that the system of equations (19) and (20) in linearized form is

$$\frac{du_{py}}{dx} = L_{12}u_{pz} + L_{14}u_{hz}, \tag{32a}$$

$$\frac{du_{pz}}{dx} = L_{21}u_{py} + L_{23}u_{hy}, \tag{32b}$$

$$\frac{du_{hy}}{dx} = L_{32}u_{pz} + L_{34}u_{hz}, \tag{32c}$$

$$\frac{du_{hz}}{dx} = L_{41}u_{py} + L_{43}u_{hy}, \tag{32d}$$

https://doi.org/10.1017/S0022377802001745 Published online by Cambridge University Press

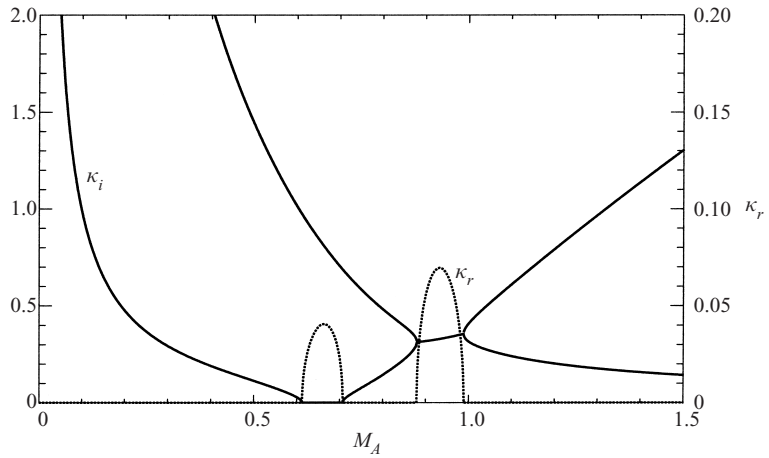

Figure 3. The real (dotted curves) and imaginary (solid curves) parts κ as a function of Alfv́en Mach number M_A in a bi-ion plasma with $\alpha = 0.1$, $\mu = 10$ and $\theta = 30°$. In the range $\sim 0.61 < M_A < 0.71$, where κ is real, evanescent solutions (which give rise to solitons) exist. In the range $0.88 < M_A < 0.99$, where κ is complex, an 'oscilliton' solution exists.

where L_{jk} are the matrix elements. Differentiating (32a) and (32c) yields

$$\frac{d^2 u_{py}}{dx^2} = a u_{py} + b u_{hy}, \tag{33a}$$

$$\frac{d^2 u_{hy}}{dx^2} = c u_{py} + d u_{hy}, \tag{33b}$$

where

$$a = L_{12}L_{21} + L_{14}L_{41}, \qquad b = L_{12}L_{23} + L_{14}L_{43},$$
$$c = L_{32}L_{21} + L_{34}L_{41}, \qquad d = L_{32}L_{23} + L_{34}L_{43}.$$

Similar equations are obtained for the z components of the proton and heavy-ion speeds. The fact that the equations for the y and z components are decoupled corresponds to the reduction of the quartic equation to a biquadratic. Equations (33) describe two coupled oscillators for u_{py} and u_{hy} (if a and $d < 0$):

$$\left(\frac{d^2}{dx^2} - a\right) u_{py} = b u_{hy}, \tag{34a}$$

$$\left(\frac{d^2}{dx^2} - d\right) u_{hy} = c u_{py}, \tag{34b}$$

or

$$\left(\frac{d^2}{dx^2} - d\right)\left(\frac{d^2}{dx^2} - a\right) u_{py} = bc u_{py}, \tag{35}$$

with similar equations for coupled oscillators for u_{pz} and u_{hz}. Exponential solutions $\sim \exp(\kappa x)$ yield a quadratic equation for κ^2:

$$(\kappa^2 - d)(\kappa^2 - a) = bc, \tag{36}$$

which has solutions

$$\kappa_{1,2}^2 = \tfrac{1}{2}[(a + d) \pm \sqrt{(a - d)^2 + 4bc}]. \tag{37}$$

https://doi.org/10.1017/S0022377802001745 Published online by Cambridge University Press

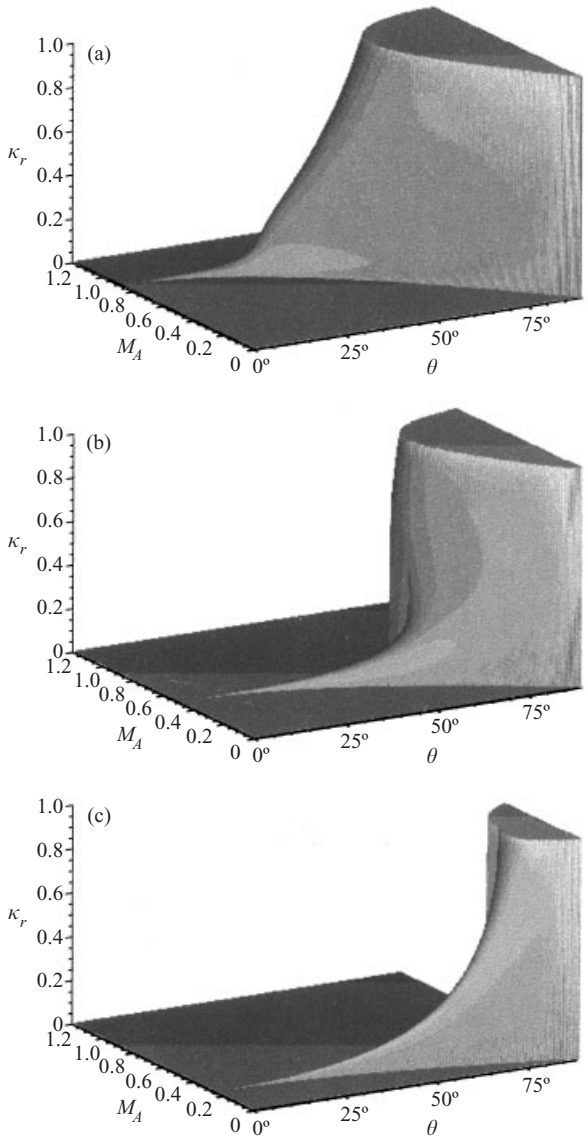

Figure 4. The regions in the (M_A, θ) plane where soliton solutions may exist in a bi-ion plasma with $\mu = 15$ and $\alpha = 0.02$ (a), 0.02 (b) and 1 (c). These three-dimensional diagrams show the real part of κ as a function of M_A and θ.

Hence κ may be real (evanescent solutions, growing or decaying), imaginary (periodic solutions), or complex (growing or decaying solutions with superimposed oscillations).

Figure 3 shows the real (dotted curves) and imaginary (solid curves) parts of κ as a function of Alfvén Mach number M_A in a bi-ion plasma with $\alpha = 0.1$, $\mu = 10$ and $\theta = 30°$ (note that here we have renormalized κ to Ω_p/V_{Ap}). For most values of M_A, the solutions are periodic. However, in the case where $\sim 0.61 < M_A \lesssim 0.71$, we find evanescent solutions that can give rise to soliton solutions if nonlinearity can be balanced by dispersion effects. Another interesting class of solutions may be

https://doi.org/10.1017/S0022377802001745 Published online by Cambridge University Press

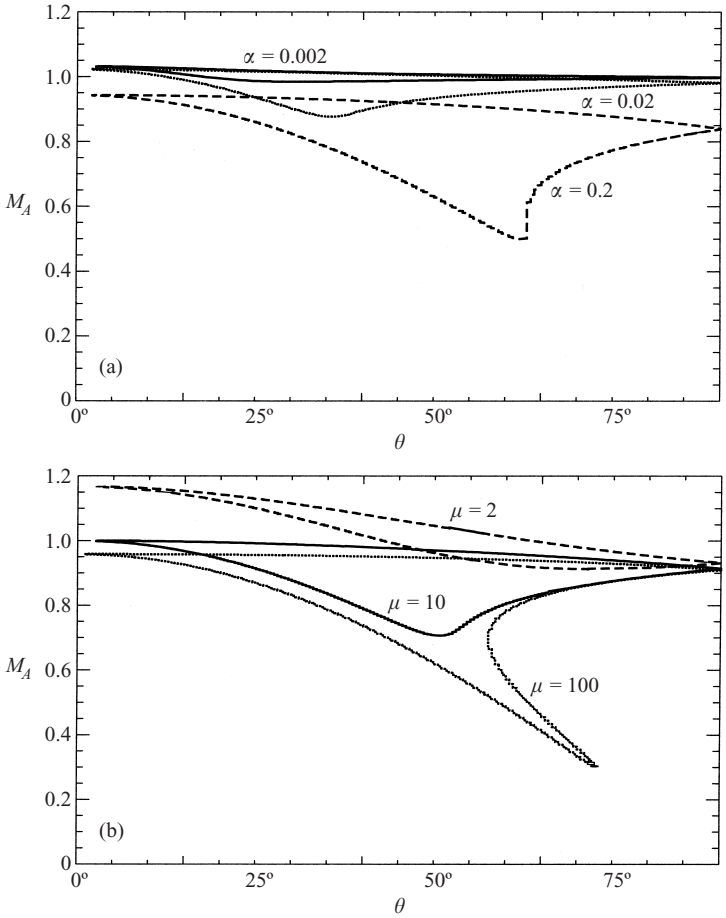

Figure 5. The regions in the (M_A, θ) plane in which oscilliton solutions may exist: (a) $\mu = 15$ and $\alpha = 0.002, 0.02, 0.2$; (b) $\alpha = 0.1$ and $\mu = 2, 10, 100$.

expected in the $\sim 0.88 < M_A \lesssim 0.99$, where κ is complex. This type of solution, characterized by an oscillating structure superimposed on the spatial growth or decay, may be called an 'oscilliton' (Sauer et al. 2001, 2002a, b).

Figure 4 shows the regions in the (M_A, θ) plane where soliton solutions may exist in bi-ion plasma with $\mu = 15$ and $\alpha = 0.02, 0.2$ and 1. The real part of κ is given along the vertical axis. For solitons propagating at small angles with respect to the magnetic field, the range of 'permitted' Alfvén Mach numbers is very narrow and the inverse growth length κ is very small. There are no soliton solutions at very small angles. An increase in the propagation angle broadens the region where solitons may exist and the growth length ($\sim 1/\kappa$) decreases. The width of the window of existence and κ_r increase sharply at a certain angle, whereas an increase in the density ratio α yields small soliton speeds at intermediate angles.

Figure 5 illustrates the regions in the (M_A, θ) plane in which oscilliton solutions may exist. At small abundances, the window of existence is very narrow. An increase in α broadens the window. At small and large angles, the range of Mach numbers M_{Ap} for oscillitons occurs at smaller values than at intermediate angles. An

https://doi.org/10.1017/S0022377802001745 Published online by Cambridge University Press

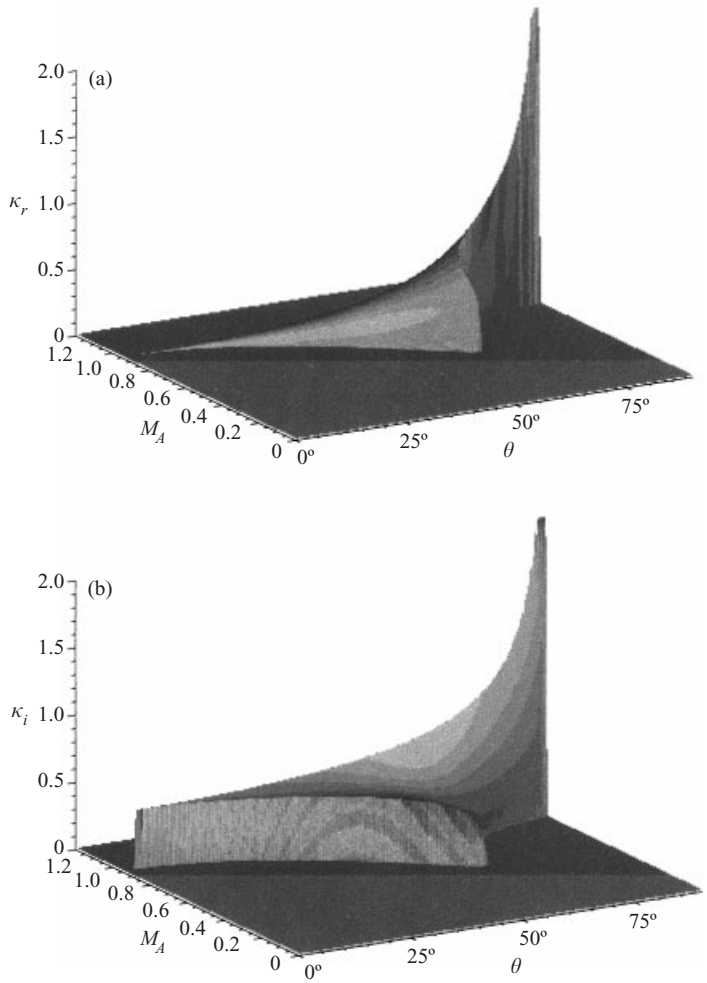

Figure 6. The regions in the (M_A, θ) plane in which oscilliton solutions may exist for $\alpha = 0.2$ and $\mu = 15$. The vertical axis gives the real part κ_r (which characterizes the spatial growth rate) in (a) and the imaginary part κ_i (the wavenumber of the oscillatory structure) in (b).

increase in the mass also yields broader windows. The interesting features is that with increasing μ, two velocity intervals for oscillitons appear at certain propagation angles. Figure 6 shows the variation of the real part κ_r (which characterizes the spatial growth rate) and the imaginary part κ_i (the wavenumber of oscillatory structure) with θ and Alfvén Mach number. As in the case of soliton-type solutions, the inverse growth length increases with the propagation angle. The wavenumber of oscillations embedded in the exponentially growing (or decaying) structure is larger at higher speeds and propagation angles.

5. Examples of solitons and oscillitons

In contrast to stationary solutions (solitons and nonlinear periodic waves) propagating transverse to the magnetic field (where, by using the conservation laws of

https://doi.org/10.1017/S0022377802001745 Published online by Cambridge University Press

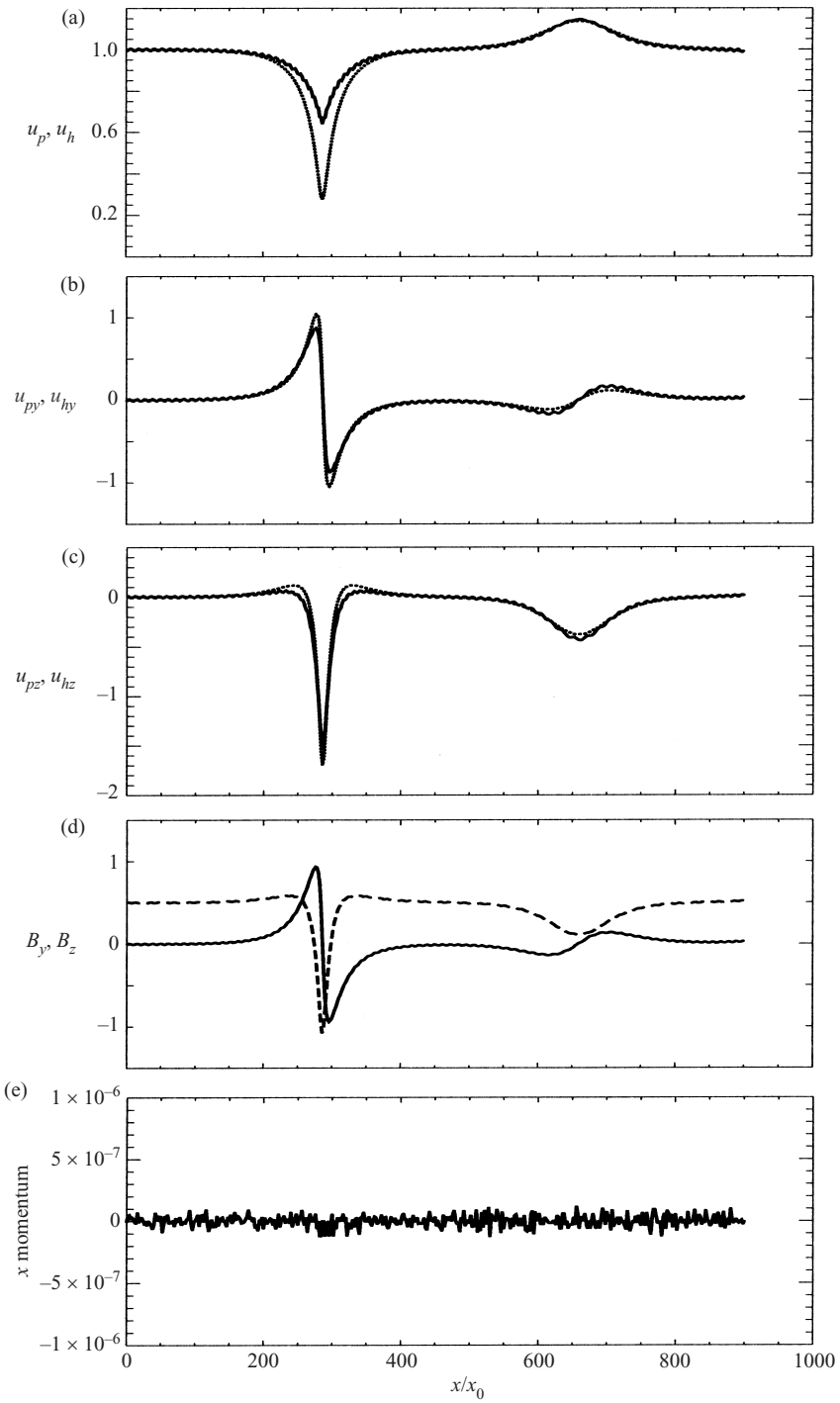

Figure 7. For caption see page 40.

https://doi.org/10.1017/S0022377802001745 Published online by Cambridge University Press

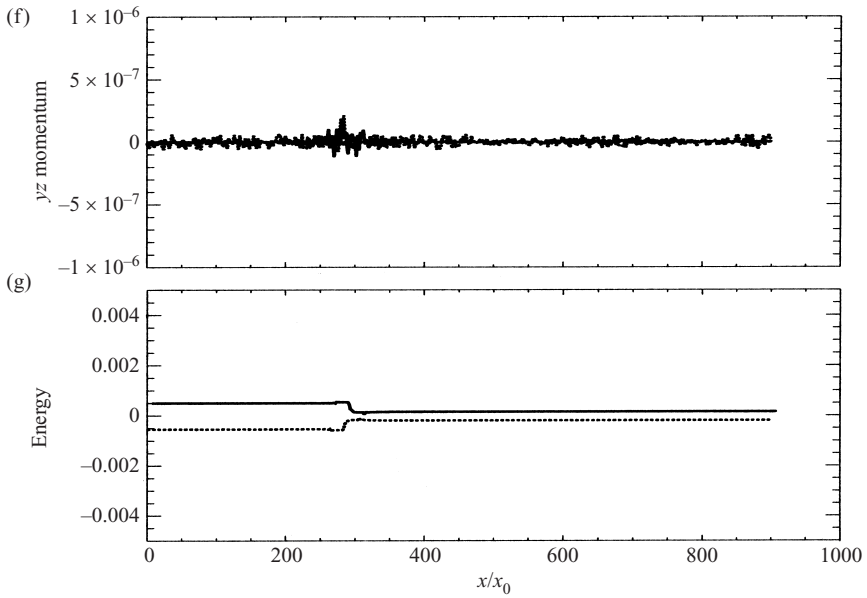

Figure 7. The structure of compressive and rarefactive solitons propagating at an angle $\theta = 30^\circ$ in a bi-ion plasma ($\alpha = 0.1$ and $\mu = 10$) streaming with $M_{Ap} = 0.65$.

a bi-ion flow, the system may be described by a first-order differential equation) (Dubinin et al. 2002), the oblique case requires the solution of the full system of four coupled differential equation. By using the 'difference energy integral', the number of differential equations may be reduced to three, but the method of analysis of phase portraits of the system cannot be applied, and therefore one must resort to numerical studies guided by our momentum–energy hodograph picture. Figure 7 shows the structure of solitons propagating at an angle $\theta = 30^\circ$ in a bi-ion plasma ($\alpha = 0.1$ and $\mu = 10$) streaming with $M_{Ap} = 0.65$. Figures 7(a–c) depict the velocities of the proton and heavy-ion flows (three components). Solid (dotted) curves correspond to the protons (heavies). Figure 7(d) shows the B_y and B_z components of the magnetic field (solid and dashed curves). Solutions contain both type of solitons – compressional and rarefactional. In the compressive soliton, the heavies run behind the protons and are decelerated down to a speed of about 0.3 at the centre of the structure. The protons slow down to about 0.67. Both flows are strongly deflected in the $-z$ direction, with $u_{pz} \approx u_{hz} \approx -1.7$. The y component of the velocity and B_y are odd functions of x. The B_z component changes sign and reaches a value of about -1.1.

The structure of the rarefactive soliton is smoother. Both fluids move with almost the same speed in the x direction. The y components of the flows and the magnetic field show a sequence of sign reversals opposite to that of the compressive solitons. Note also the small-amplitude oscillations (nonlinear periodic waves), which can be expected from the dispersion diagram for stationary waves shown in Fig. 3. These oscillations correspond to another mode with $\kappa \approx 0.9$. The curves in Figs 7(e–g) test conservation of the momentum fluxes in the x, y and z directions (solid and dotted curves respectively), and the changes in the energy flux (solid curve) and 'difference energy density' (dotted curve). The conservation of these quantities gives creditability to the numerical solutions.

https://doi.org/10.1017/S0022377802001745 Published online by Cambridge University Press

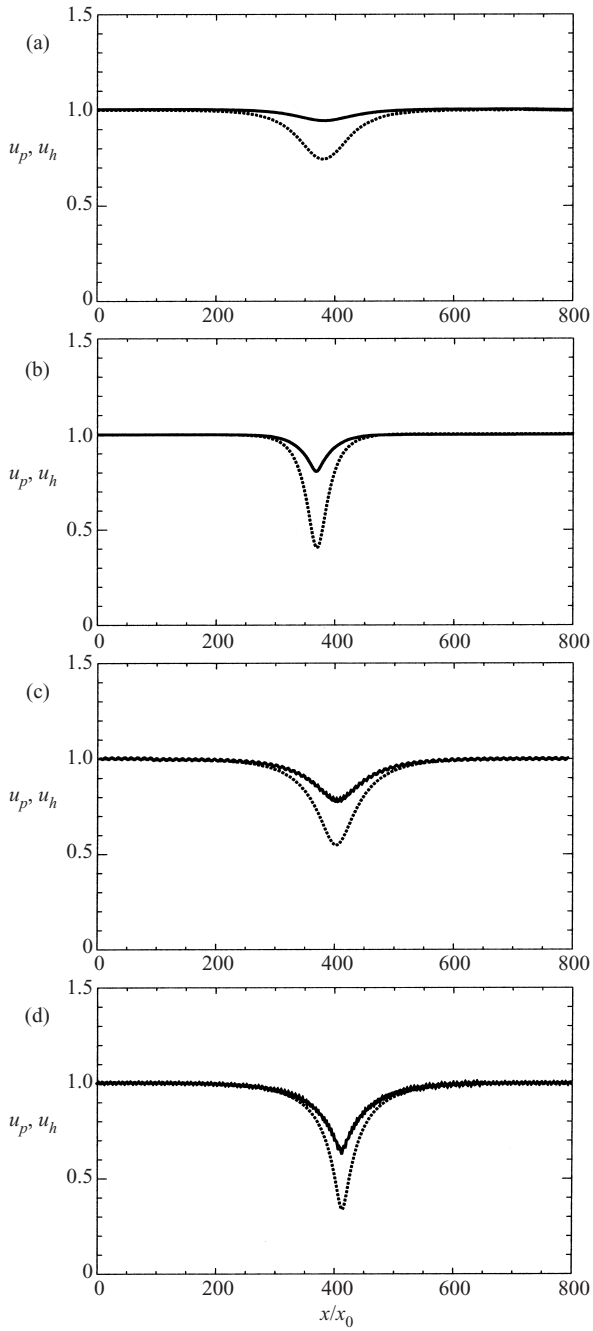

Figure 8. Solitons propagating at $\theta = 30°$ in a bi-ion plasma with $m_h/m_p = 10$, for different abundances α of the heavies: (a) $\alpha = 0.001$, $M_A = 0.863$; (b) $\alpha = 0.01$, $M_A = 0.84$; (c) $\alpha = 0.1$, $M_A = 0.63$; (d) $\alpha = 1$, $M_A = 0.28$.

The structure of compressive solitons is insensitive to the density ratio $\alpha = n_{h0}/n_{p0}$ (only the soliton speed varies). This is not suprising, since the radius of the momentum–energy sphere along which the bi-ion system evolves depends only on the propagation angle.

https://doi.org/10.1017/S0022377802001745 Published online by Cambridge University Press

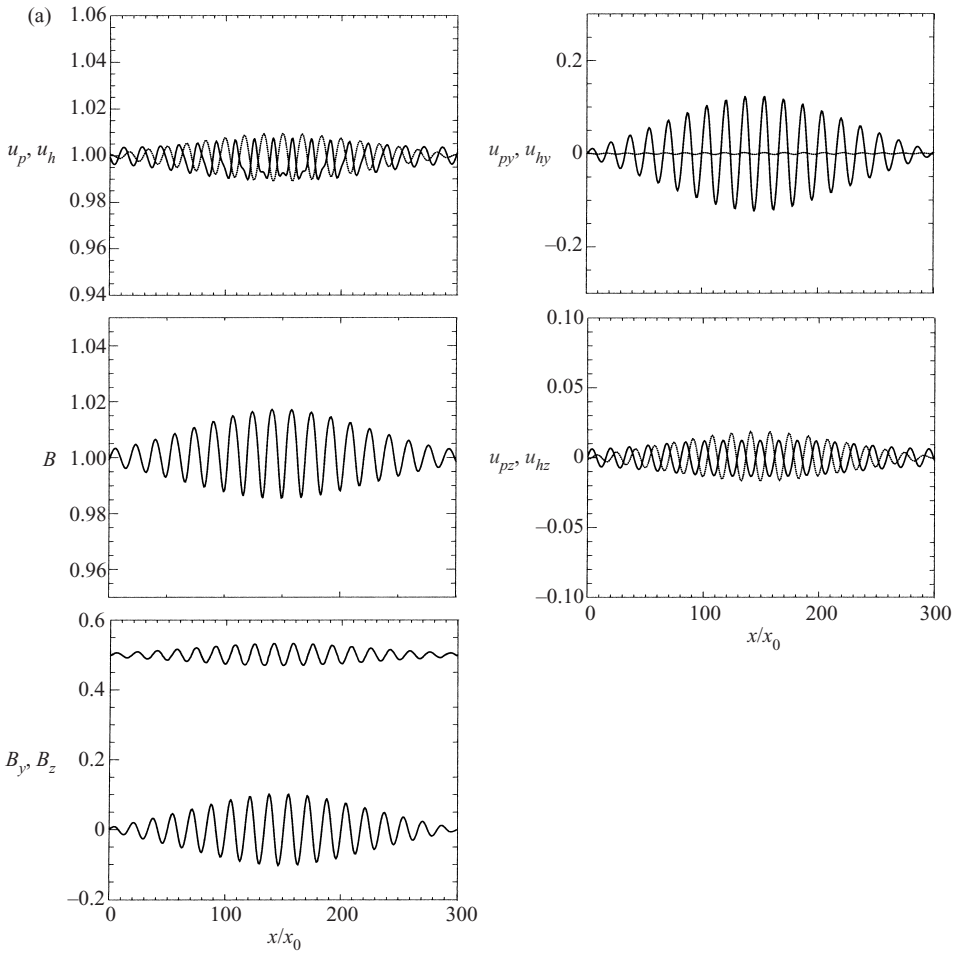

Figure 9. For caption see facing page.

Figure 8 shows examples of solitons propagating at $\theta = 30°$ in a bi-ion plasma with $m_h/m_p = 10$ and $\alpha = 0.001$, 0.01, 0.1 and 1. In all cases, the heavies (dotted curves) lag behind the protons (solid curves). The only important difference is the range of flow speeds where soliton solutions can be constructed.

Figure 9 gives some examples of oscillitons. Figure 9(a) shows how the dynamical variables vary in an oscilliton propagating in a bi-ion plasma ($\alpha = 0.2$ and $\mu = 15$) at $\theta = 30°$. The flow speed ($M_{Ap} = 0.827$) is close to the lower border of the velocity interval, where κ is complex and the oscilliton has a rather symmetrical wavepacket shape. Oscillations in the proton and heavy-ion flow in the x and z directions are clearly shifted in phase. The wavelength of the oscillations is close to the value of κ_i determined from the dispersion equation for stationary waves. However, an increase in the Mach number (Fig. 9b) breaks the coherence of the wave (the real part κ_r begin to dominate over the imaginary part κ_i) and oscilliton structure resembles a soliton with superimposed oscillations. Higher and higher harmonics appear with increasing Mach number. A critical Mach number may be reached where $u_{hx} \to 0$ and smooth oscilliton solutions can no longer be constructed.

https://doi.org/10.1017/S0022377802001745 Published online by Cambridge University Press

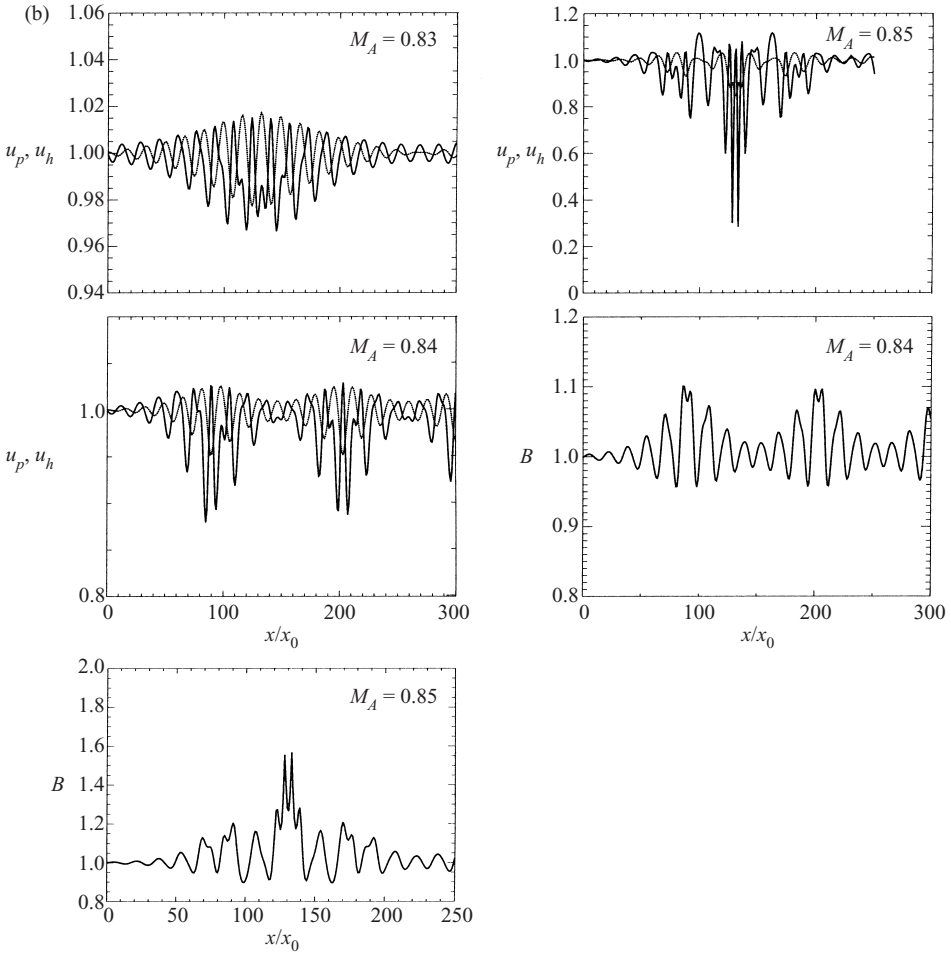

Figure 9. (a) Structure of an oscilliton propagating in a bi-ion plasma ($\alpha = 0.2$ and $\mu = 15$) at $\theta = 30°$ with a speed ($M_{Ap} = 0.827$) close to the lower border of the velocity interval where oscillitons may exist. (b) Evolution of oscillitons with increasing Mach number. A small increase in M_A breaks a wavepacket. Solid curves are for protons; dotted curves are for heavies.

6. Critical Mach numbers

Figure 10(a) shows the structure of compressional solitons at different Alfvén Mach numbers. As M_{Ap} increases from 0.62 to 0.68 ($\alpha = 0.1$, $\mu = 10$ and $\theta = 30°$), the compression ($1/u_{ix}$) of the heavies (protons) is enhanced by 7.2 (1.7). At $M_{Ap} = 0.686$, the compression in the heavy-ion flow reaches about 20. The critical Mach number corresponds to a 'stagnation' point of the heavies ($u_{hx} \to 0$), while the proton speed remains finite. Figure 10(b) gives examples of rarefaction solitons at different Alfvén Mach numbers in the same range of speeds that show a different behaviour from the compressive case. The amplitude of the soliton (maximum expansion) reaches a maximum value at $M_{Ap} \approx 0.65$ and then decreases, vanishing smoothly at a value of M_{Ap} determined by the necessary condition for soliton existence (real positive κ) (see Fig. 3). Also, the difference between the proton and heavy-ion speeds u_{px}

https://doi.org/10.1017/S0022377802001745 Published online by Cambridge University Press

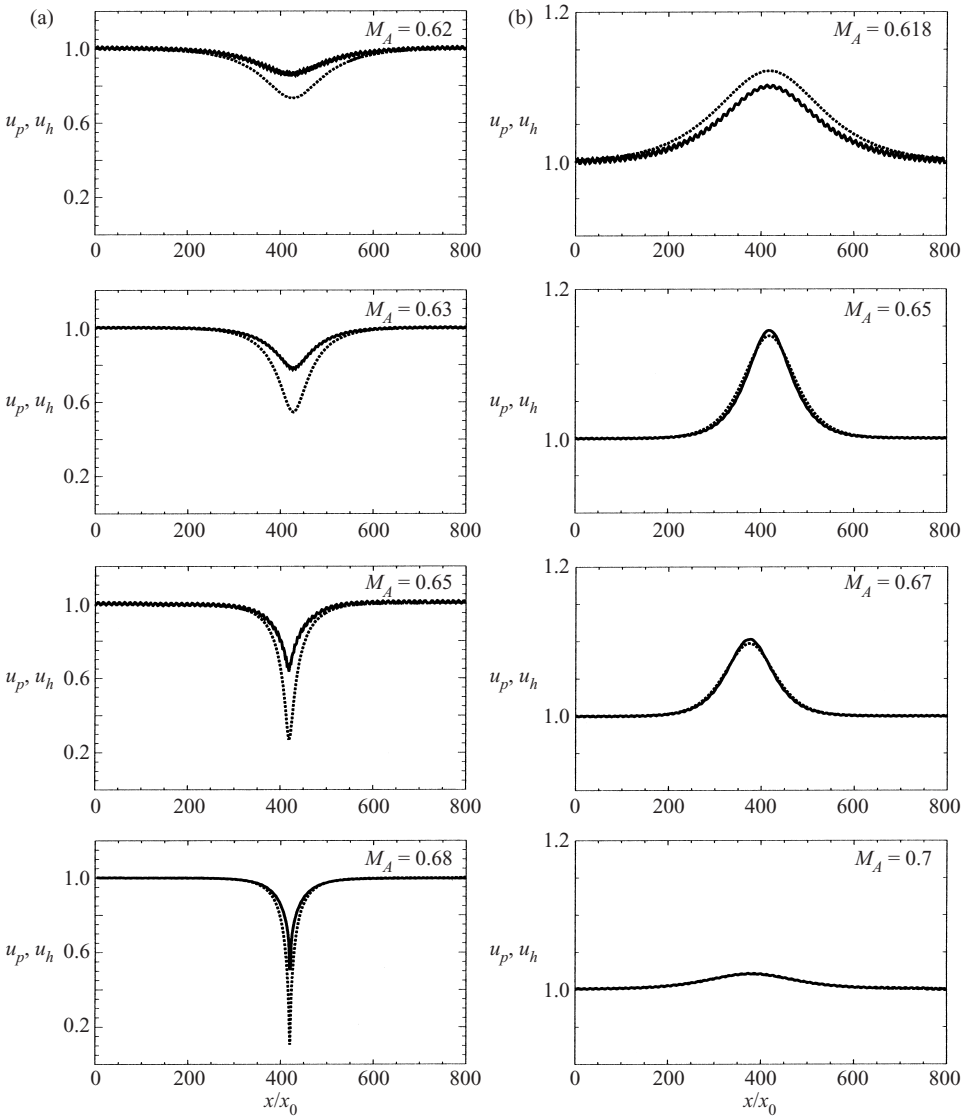

Figure 10. (a) Structure of compressional solitons at different Alfvén Mach numbers propagating at $\theta = 30°$. (b) Structure of rarefactive solitons as a function of the Alfvén Mach number in the same range of Mach numbers. $\alpha = 0.1$ and $\mu = 10$. Solid curves are for protons; dotted curves are for heavies.

and u_{hx} is small, but becomes larger at more oblique angles. Figure 11 shows the structure of the rarefaction solitons propagating at 80° with respect to the magnetic field. The protons lag strongly behind the heavies, and the expansion in the heavy-ion flow reaches about one-sixth, while the proton number density only goes down to about two-thirds.

It is interesting to consturct the momentum-energy hodographs near the critical Mach numbers as in Fig. 12, which shows the three characteristic curves (the momentum flux, energy flux and energy density difference relation) in the (u_{hx}, u_{px})

https://doi.org/10.1017/S0022377802001745 Published online by Cambridge University Press

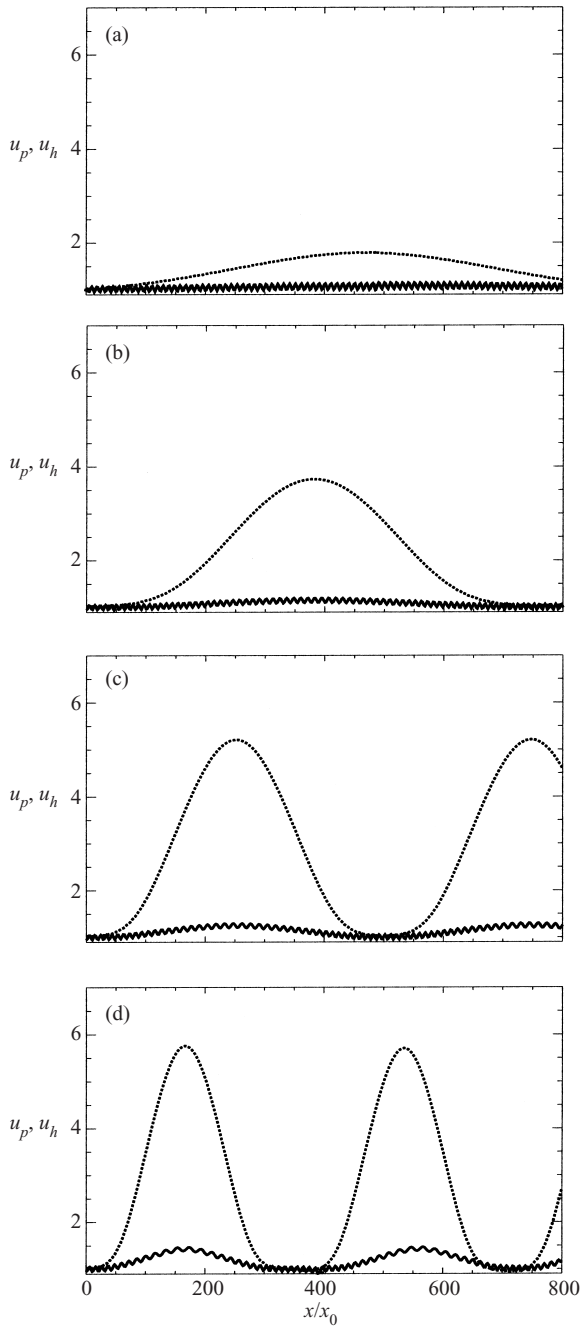

Figure 11. Structure of rarefactive solitons propagating at 80° with respect to the magnetic field for $\alpha = 0.1$ and $\mu = 10$: (a) $M_A = 0.123$; (b) $M_A = 0.125$; (c) $M_A = 0.13$; (d) $M_A = 0.138$. Solid curves are for protons; dotted curves are for heavies.

plane as M_A increases for $\alpha = 0.2$, $\mu = 15$ and $\theta = 30°$. The intersection point C, which goes to the left ($u_h \to 0$), corresponds to the state of maximum amplitudes (the centres of the solitons). Since R_3^2 (see (25c)) changes sign, the hyperbola (energy density relation) switches to other quadrants (at $M_{Ap} = 0.48$) and the point

https://doi.org/10.1017/S0022377802001745 Published online by Cambridge University Press

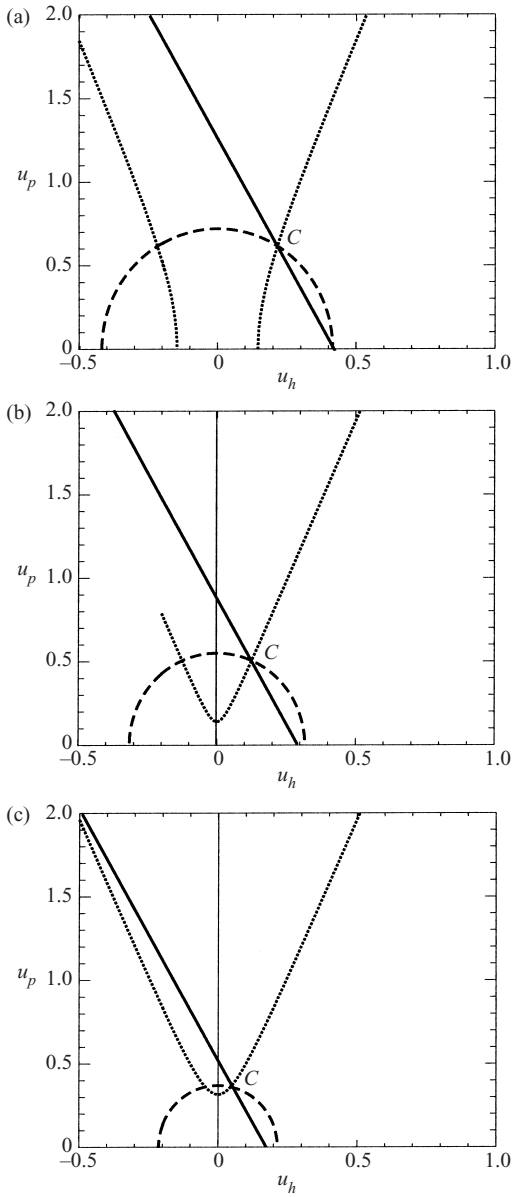

Figure 12. The three characteristic curves (the momentum flux, energy flux and energy density difference relation) in the (u_{hx}, u_{px}) plane at $M_A = 0.47$ (a), 0.48 (b) and 0.488 (c). At some critical Mach number, when the energy flux and energy density curves have double contact, u_{hx} goes to zero while a finite compression remains in the proton flow.

C moves closer to the u_{px} axis. At some critical Mach number, u_{hx} goes to zero while a finite compression remains in the proton flow. At this point, the z component of the heavy flow reaches its maximum value, determined from the quadratic equation (24) for $u_{hx} = 0$ and $u_{hy} = 0$: $u_{hz} = -E_y/B_x - \sqrt{1 + E_y^2/B_x^2}$. Note also that the energy flux and energy density curves have double contact at this point.

https://doi.org/10.1017/S0022377802001745 Published online by Cambridge University Press

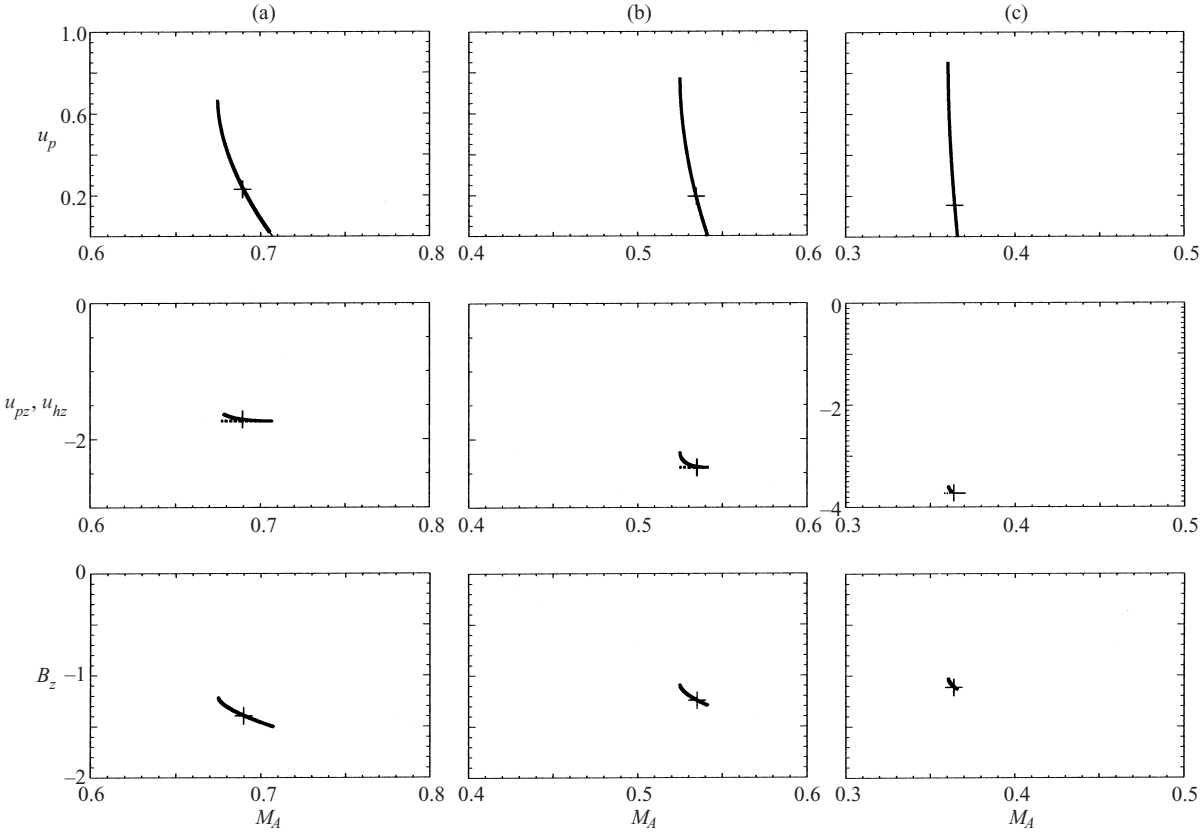

Figure 13. Families of critical amplitudes for possible soliton solutions value for $\alpha = 0.1$, $\mu = 10$ and $\theta = 30^\circ$ (a), 45° (b) and 60° (c). The actual critical values can only be obtained by solving the differential equations. Crosses on the curves indicate these values. The upper limit of these critical Alfvén numbers corresponds to stagnation of both fluids ($u_{px} = 0$, $u_{hx} = 0$). In the u_{pz} and u_{hz} plots, solid curves are for protons and dotted for heavies.

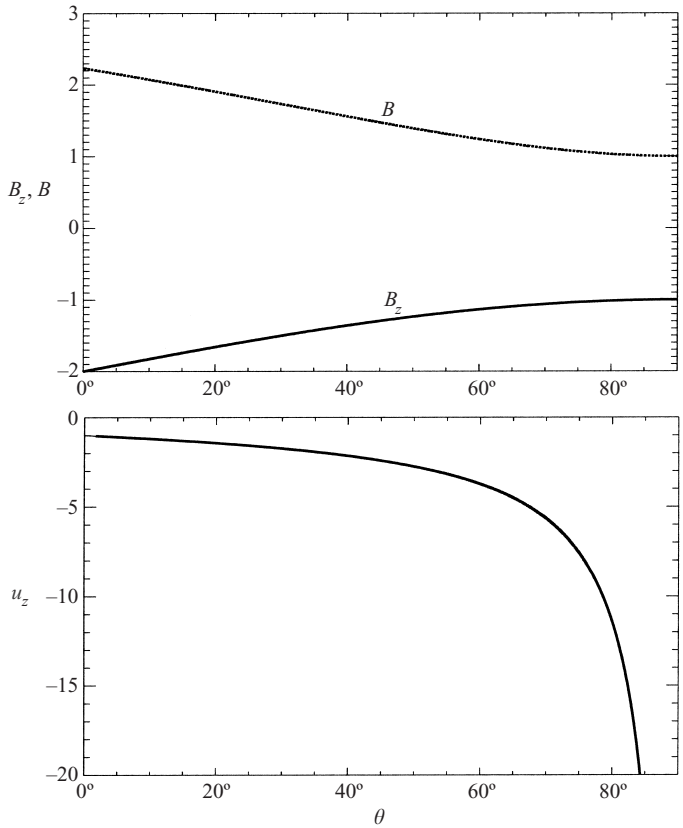

Figure 14. Critical amplitudes (B_z, B, u_z) of solitons at the upper critical Mach numbers as functions of the propagation angle θ for $\alpha = 0.1$ and $\mu = 10$.

To obtain the remaining critical values (the variables u_{px}, u_{pz}, B_z and $M_{A\mathrm{cr}}$ at a fixed angle θ; u_{py}, u_{hy} and B_y are zeros at the centre of the soliton) we have only three constants of motion:

$$u_{px} - 1 - \alpha\mu + \frac{B_z^2 - B_{z0}^2}{2M_{A\mathrm{cr}}^2} = 0, \tag{38a}$$

$$u_{pz} + \alpha\mu u_{hz} - \frac{B_x(B_z - B_{z0})}{M_{A\mathrm{cr}}^2} = 0, \tag{38b}$$

$$u_{px}^2 - 1 + u_{pz}^2 + \frac{2E_y u_{pz}}{B_x} = 0, \tag{38c}$$

which assumes a continuous family of solutions. Figure 13 shows families of critical values for possible soliton solutions at different θ for $\alpha = 0.1$ and $\mu = 10$. The actual critical values can be obtained by solving the differential equations. Crosses on the curves give these values. Note that the upper limit of the critical Alfvén numbers corresponds to $u_{px} = 0$, i.e. stagnation of both fluids. The amplitude of such 'critical

https://doi.org/10.1017/S0022377802001745 Published online by Cambridge University Press

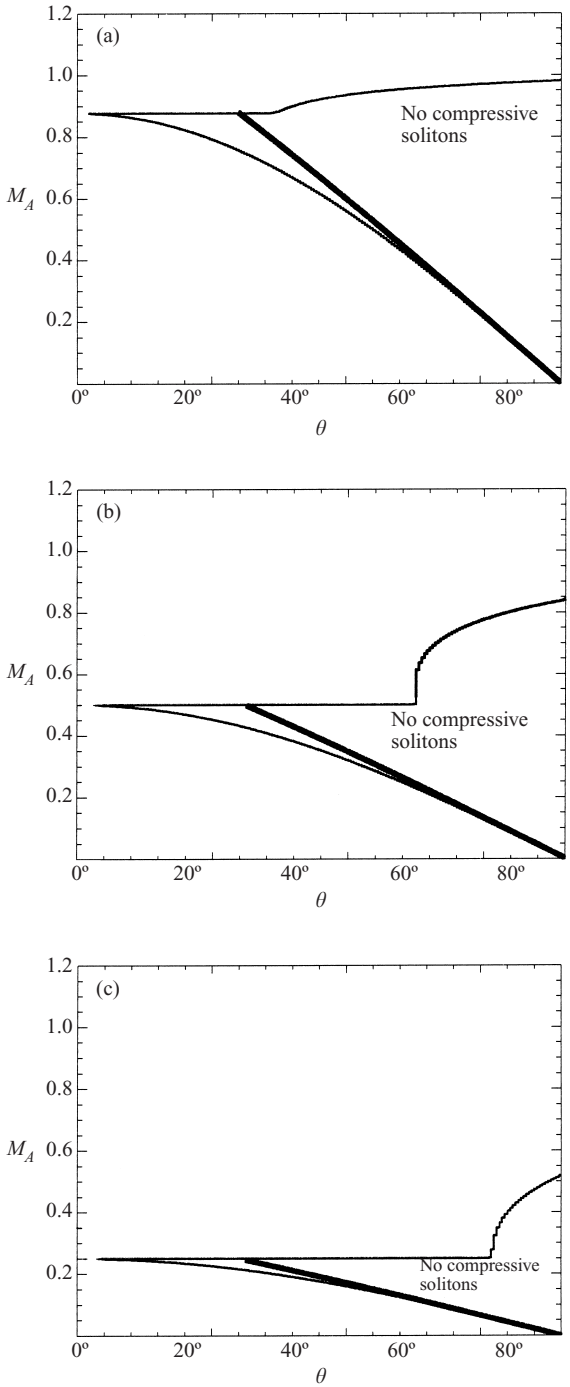

Figure 15. The regions in the (M_A, θ) plane where soliton solutions may exist in bi-ion plasma with $\mu = 15$ and $\alpha = 0.02$ (a), 0.2 (b) and 1 (c) (see also Fig. 4). Thick solid lines show the upper limit of critical Mach numbers for compressive solitons (at different propagation angles). To the right of these curves smooth compressive solitons cannot exist.

https://doi.org/10.1017/S0022377802001745 Published online by Cambridge University Press

solitons' is determined only by the obliquity (the point C_m in Fig. 1):

$$u_{pz} = u_{hz} = -\frac{E_y}{B_x} - \sqrt{1 + \frac{E_y^2}{B_x^2}} \equiv U_z, \tag{39a}$$

$$B_z = \frac{2B_x}{U_z} - B_{z0}. \tag{39b}$$

Figure 14 shows how these critical amplitudes vary with θ. The upper critical Mach number is given by

$$M_{A\mathrm{cr}} = \sqrt{\frac{2B_x(B_x/U_z - B_{z0})}{(1+\alpha\mu)U_z}}. \tag{40}$$

The solid lines in Fig. 15 show the upper limit of critical Mach numbers for compressive solitons in a bi-ion plasma with $\mu = 15$ and $\alpha = 0.02$, 0.2 or 1 as a function of angle θ. Figure 15 also shows the range of parameters θ and M_{Ap} for which soliton solutions may exist. The existence of a critical Mach number significantly limits the range of speeds and angles where smooth soliton solutions can be constructed. At small angles, compressive solitons exist in the whole permitted range. At larger angles, smooth soliton solutions can be constructed only in a narrow region below the solid curve that depicts the upper critical Mach number (close to the lower border of soliton existence regions).

In rarefaction solitons, the maximum possible expansion of the heavy-ion flow is a function only of the propagation angle θ ($u_{hx} = \sqrt{1 + \tan^2\theta}$) (the top point on the momentum–energy sphere). At this point, $u_{hz} = -E_y/B_x = -\tan\theta$. For example, for $\theta = 80°$, the maximum possible expansion is $u_{hx_{\max}} \approx 5.78$ and $u_{hz} = -5.67$. In the soliton shown in Fig. 11(d), the heavy-ion flow almost attains such a rarefaction. Note that the deflection of the proton fluid ($u_{pz} \approx -11.5$) in this case is about two times stronger than that of the heavies. With a further increase in Mach number, the expansion in the heavy-ion flow decreases, although the proton expansion increases. For example, at $M_{Ap} = 0.15$ and 0.16 ($\alpha = 0.1$ and $\mu = 10$), the speeds u_{hx}, u_{px} are approximately 5.2, 2.2 and 4.5, 3.5 respectively. One may expect that a further increase in M_{Ap} will cause the proton expansion to reach a maximum value (accompanied by a small rarefaction in the heavies) and thereafter decrease.

7. Summary and conclusions

We have investigated the properties of stationary waves propagating obliquely to the magnetic field in a cold bi-ion plasma on the basis of multifluid equations. In contrast to the transverse case, where the number of variables (e.g. $u_{px}, u_{hx}, u_{py}, u_{hy}$ and B_z) equals $n+1$, with n being the number of constants of motion (current-free condition, two momentum flux constants and the energy flux integral), so that the system of equations can be reduced to a single first-order differential equation, in the oblique case, the number of variables (e.g. $u_{px,py,pz}, u_{hx,hy,hz}, B_y$ and B_z) equals $n + 4$. Here the constants of motion are three momentum fluxes and the energy flux integral. Thus the total system of equations can be reduced only to four coupled first-order differential equations (e.g. for the transverse flow speeds ($u_{py}, u_{hy}, u_{pz}, u_{hz}$)), and therefore the method of phase portraits in the ($u_i, du_i/dx$) planes cannot be usefully applied.

Nevertheless, several interesting properties of stationary waves can be found

https://doi.org/10.1017/S0022377802001745 Published online by Cambridge University Press

without solving these differential equations. In fact, we have found an additional constant of motion, which we call the energy difference integral because it relates changes in kinetic energy of the heavy ions and the protons in a stationary flow. This, together with the energy flux constant, yields another pair of constants of motion, (23) and (24), permitting a simple geometrical interpretation. Throughout any bi-ion stationary flow, the tip of the proton (heavy-ion) flow velocity vector moves on the surface of a sphere of radius $R_E = \sqrt{1 + E_y^2/B_x^2}$, displaced from the origin along the $u_{pz,hz}$ axis by $-E_y/B_x$ units. Downward or upward motions from the initial point $(1, 0, 0)$ correspond to compressive or rarefactive flows respectively. The actual trajectories of the p, h tips along the spherical surface, however, can only be found by solving the coupled system of differential equations.

In the neighbourhood of the initial point, where linearization of the differential equations is legitimate, the motions of the two ion fluids in the y and z directions become decoupled and the system of equations is reduced to two pairs of equations describing two pairs of coupled oscillators (for the y and z speeds). These equations determine the range of Alfvén Mach numbers in which evanescent (exponentially growing or decaying) solutions (and hence solitons) exist. 'Windows' in the (M_A, θ) plane in which soliton solutions may exist (the necessary condition for their existence) vary with the abundance ratio of the heavies $\alpha = n_{h0}/n_{p0}$ and the mass ratio $\mu = m_h/m_p$. An interesting feature is that solitons in a bi-ion plasma cannot propagate at very small angles to the ambient magnetic field. In addition to solitons, another type of stationary solution called 'oscillitons', characterized by an oscillating spatial structure superimposed on the spatial growth or decay, found recently by Sauer et al. (2001, 2002a, b), were studied. Oscillitons can exist at specific windows in parameter space. It is suggested that coherent wave packets often observed in multi-ion space plasmas are in fact oscillitons, i.e. structures with both oscillating and soliton properties.

An increase in the Alfvén Mach number (at a fixed angle of propagation) or an incease in the angle θ (at a fixed Mach number) may cause the amplitude of a compressive soliton to reach a critical value before the upper boundary of the soliton existence region in the (M_A, θ) plane is reached. Such a critical Mach number corresponds to 'stagnation' of the heavy-ion flow ($u_{hx} \to 0$), accompanied by its greatest deflection, while a finite compression of the proton flow remains. On the 'velocity sphere' of the heavies, this corresponds to a point $(0, 0, -E_y/B_x - \sqrt{1 - E_y^2/B_x^2})$ whose position is determined by obliquity. The maximum expansion also depends only on the sphere parameters $(\sqrt{1 + E_y^2/B_x^2},\ 0, -E_y/B_x)$. The structure of an oscilliton varies dramatically with Alfvén Mach number. A wave packet with almost coherent oscillations can be transformed into a strongly nonlinear wave with higher harmonics.

The inclusion of finite proton and heavy-ion pressures will introduce additional windows where solitons can be constructed because of the appearance of a new (slow) wave mode (see e.g. Hackenberg et al. 1998). In this case, critical points (where $du_i/dx \to 0$) arise, and these may intervene before equilibrium points are reached. In bi-ion plasmas, these singularities arise when ion speeds lie on certain stationary wave loci of Mach numbers (McKenzie et al. 1993; Dubinin et al. 2002). For waves propagating transverse to the magnetic field, these loci can be found by analysing the denominator of the first-order structure equation. In the oblique

case, the dynamics of a bi-ion system becomes more complicated, since the system is described by four coupled first-order differential equations.

Acknowledgements

E.D. thanks the Deutsche Forschungsgemeinschaft and the Max-Planck-Gesellschaft for supporting this work by grants. The work was also supported by a grant INTAS-ESA-99-00066.

References

Dubinin, E. M., Sauer, K., McKenzie, J. F. and Chanteur, G. 2002 Nonlinear waves and solitons propagating perpendicular to the magnetic field in bi-ion plasma with finite plasma pressure. *Nonlinear Processes Geophys.* **9**, 87.

Hackenberg, P., Mann, G. and Marsch, E. 1998 Solitons in multi-ion plasmas. *J. Plasma Phys.* **60**, 845.

McKenzie, J. F. and Doyle, T. B. 2001 Oblique solitons in a cold magnetized plasma. *Phys. Plasmas* **8**, 4367.

McKenzie, J. F., Marsch, E., Baumgartel, K. and Sauer, K. 1993 Wave and stability properties of multi-ion plasmas with applications to winds and flows. *Ann. Geophys.* **11**, 341.

McKenzie, J. F., Sauer, K. and Dubinin, E. 2001 Stationary waves in a bi-ion plasma transverse to the magnetic field. *J. Plasma Phys.* **65**, 197.

Sauer, K., McKenzie, J. F. and Dubinin, E. 2000 Waves and nonliner structures in bi-ion plasmas. In: *Waves in Dusty, Solar and Space Plasmas* (ed. F. Verheest, M. Goossens, M. A. Hellberg and R. Bharuthram). Woodhead, NY: American Institute of Physics Conference Proceedings Series, p. 327.

Sauer K., Dubinin, E. and McKenzie, J. F. 2001 New type of soliton in bi-ion plasmas and possible implications. *Geophys. Rev. Lett.* **28,** 3589.

Sauer K., Dubinin, E. and McKenzie, J. F. 2002a. Coherent waves in multi-ion plasmas. *Physica Scripta* **T98**, 52.

Sauer K., Dubinin, E. and McKenzie, J. F. 2002b Solitons and oscillitons in multi-ion space plasmas. *Nonlinear Processes Geophys.* (in press).

Verheest, F. 1990 Nonlinear parallel Alfvén waves in cometary plasmas. *Icarus* **86**, 273.